Progress In Electromagnetics Research M, Vol. 106, 1–14, 2021

Half-Mode Substrate Integrated Waveguide Evanescent-Mode Filters with Slots-Embedded Complementary Split-Ring Resonators for Depressed Machining Tolerance Sensitivity

Bo Wang[1] and Yong Mao Huang[2, *]

Abstract—In this paper, half-mode substrate integrated waveguide (HMSIW) bandpass filters with modified complementary split-ring resonators (CSRRs) for the reduction of machining tolerance sensitivity are presented. Profiting from the evanescent-mode resonance operation, the conventional CSRR and its modified versions have been successfully utilized to miniaturize the physical sizes of SIW components. However, few investigations have focused on the fabrication tolerance. Performance of most CSRR-loaded SIW components, as well as their modified versions, is significantly sensitive to the fabrication tolerance. Hence, as the conventional machining process is with large fabrication tolerance, the CSRR-loaded SIW components suffer from limited performance and restrained application practicability. To decrease the influence from the machining tolerance on the components' performance, slots-embedded CSRR (SECSRR) is proposed and loaded into HMSIW to design evanescent-mode filters. Numerical simulations exhibit that the proposed SECSRR can help to decrease the machining tolerance sensitivity effectively as the fractional frequency offset resulting from the fabrication error is reduced from $\pm 8.11\%$ to $\pm 4.95\%$, which indicates that the proposed SECSRR is able to improve the suitability of SIW/HMSIW components and circuits for practical radio frequency (RF) and microwave applications.

1. INTRODUCTION

The past two decades have witnessed the glorious development of substrate integrated waveguide (SIW). As an emerging guided-wave structure proposed in 1999, SIW not only maintains the advantages of conventional metallic rectangular waveguide like high quality factor, low loss, high power capacity, but also can be easily integrated with various planar transmission lines, including microstrip, coplanar waveguide, and slot line [1]. Moreover, SIW maintains quite a few advantages over conventional rectangular waveguide such as low profile, small size, easy manufacturing, and low cost. Therefore, with the aforementioned merits and advantages, SIW has been widely utilized to design various microwave and millimeter wave circuits and components, such as antennas, couplers, phase shifters, power dividers, and filters. However, owing to the inherent limitation from SIW's cut-off guided-wave wavelength, SIW components typically suffer from the terrible drawback of much larger physical sizes than their corresponding microstrip counterparts at the same frequency range, which seriously restricts the practical applications of SIW.

To overcome this disadvantage, different kinds of miniaturization techniques have been developed. In 2006, half-mode SIW (HMSIW) was developed based on the principle of equivalent magnetic wall axial symmetry [2]. With the equivalent magnetic wall cutting, the transverse dimension of SIW can

Received 11 August 2021, Accepted 1 November 2021, Scheduled 14 November 2021

* Corresponding author: Yong Mao Huang (ymhuang1988@126.com).

[1] Project Management Department, Commercial Aircraft Corporation of China Ltd, Shanghai 200126, China. [2] School of Electrical and Electronic Information, Xihua University, Chengdu 610039, China.

be reduced by nearly 50%, with only a bit of epitaxial substrate to compensate the fringing capacitance effect. Moreover, with the same mechanism, the quarter-mode SIW, eighth-mode SIW, sixteenth-mode SIW, thirty-second-mode SIW, and even sixty-fourth-mode SIW have been gradually proposed for compact filters, antennas, and filtering power dividers applications. Secondly, the physical size of SIW can also be effectively miniaturized by using the multilayer printed circuit board (PCB) process [3], which delivers folded SIW, ridged SIW, and cross-layer-coupled SIW. However, multilayered SIW usually suffers from the problems of complex fabrication and excessive loss. Last but not least, by loading various unique electromagnetic structures on SIW, an extra passband can be generated below the cut-off frequency of the main transmissible mode of SIW, which means that the physical size of SIW can be squeezed greatly. For instance, a complementary split-ring resonator (CSRR) is loaded on the top surface of SIW to construct SIW-CSRR unit cell, which can realize evanescent mode transmission [4]. This impressive study has inspired plenty of further investigations on the combination of SIW and CSRR for the implementation of various microwave components. Currently, the conventional CSRR and its many modification versions have been loaded into different SIW structures to design various compact components. Meanwhile, a novel cross-coupled complementary split-ring resonator is developed and loaded into SIW to realize compact filter in [5]. It has been figured out that, in the octave band of the center frequency, there is no spurious response corresponding to the higher-order resonant mode of the resonator. Furthermore, in [6], a novel dual-band reconfigurable antenna is reported, which is capable of dual-band operation by loading an electrically small CSRR structure. In 2021, compact triple-band and quad-band SIW power dividers based on unequal CSRRs and U-shaped slots are developed [7]. Experiment results show that the proposed power divider prototypes exhibit attractive performance in terms of multiband operation, compact size, good return loss, and high isolation. Above all, loading CSRR and its modification versions has been clarified as one of the most impressive methods to realize size miniaturization of SIW circuitry.

However, by summarizing the literatures, there is an ignored issue that the CSRR structure is quite sensitive to the fabrication tolerance, which will result in non-negligible inaccuracy on the overall performance of the SIW-CSRR unit cell. More seriously, for the modification versions of CSRR and SIW, their frequency response will typically be much more sensitive to the fabrication tolerance. Furthermore, using the conventional machining process will even worsen this tolerance sensitivity. Generally, the inherent fabrication tolerance of machining process will influence the size accuracy of CSRR, and consequently cause the resonant frequency and transmission zero location of SIW-CSRR unit cell shifting higher or lower. Moreover, the operation bandwidth, selectivity and out-of-band rejection might also be influenced by the machining tolerance. Hence, under such situation, the potential components applications of SIW-CSRR structures are limited. Meanwhile, during the past two decades, investigations seldom focused on the fabrication and machining tolerance sensitivity of SIW components, which is highly demanded in future wireless applications enabled by SIW technology.

Based on the aforementioned analyses, a slots-embedded CSRR (SECSRR) is proposed and loaded into HMSIW to constitute evanescent-mode filters in this work. First of all, the embedded stub slots can help to effectively enhance the equivalent capacitance and inductance of conventional CSRR, thus to achieve size miniaturization. Secondly, more significantly, the embedded stub slots are useful to decrease the machining tolerance sensitivity of conventional CSRR, so that to improve the fabrication robustness of the proposed HMSIW-SECSRR evanescent-mode filters. In this way, the resonance frequency offset of the proposed filters can be decreased effectively. This paper is arranged as follows: Section 2 discusses the proposed SECSRR and its integration with conventional HMSIW, including numerical analyses on the decreased machining tolerance sensitivity. Section 3 describes the detailed experiments and brief discussions of the proposed HMSIW-SECSRR filters, and a conclusion is given finally.

2. HMSIW-SECSRR UNIT CELL

2.1. Resonance Properties

Figure 1 shows topologies of the conventional CSRR and proposed SECSRR. It can be easily obtained that the proposed SECSRR mainly consists of the conventional CSRR and several stub slots. Here, the ellipsis denotes that the number of stub slots embedded at each side of CSRR can be variable depending on the specific demands of practical applications. Moreover, all the embedded stub slots are unscaled,

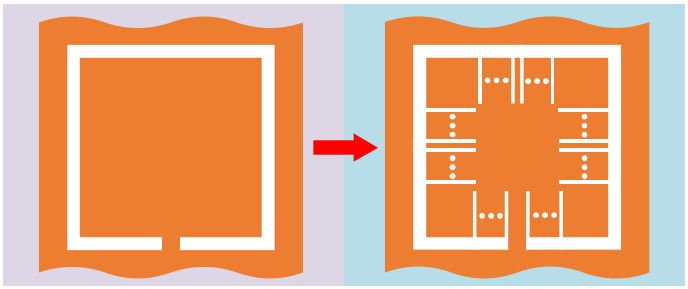

(a) (b)

Figure 1. Topologies of the conventional CSRR and the proposed SECSRR. (a) CSRR; (b) SECSRR.

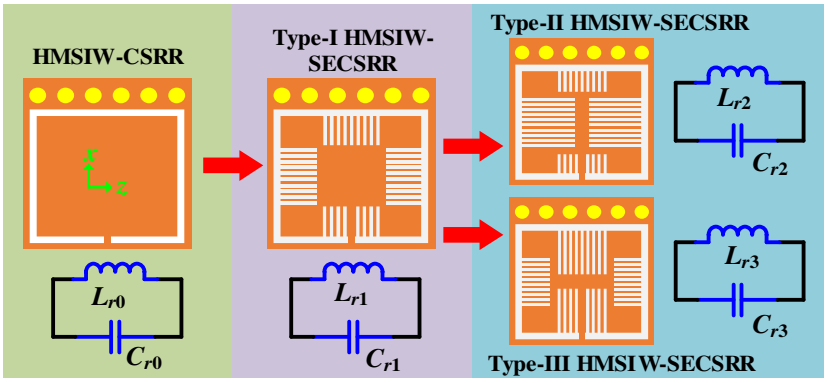

Figure 2. Derivation process from HMSIW-CSRR unit cell to various HMSIW-SECSRR unit cells.

which means that the length and width of the stub slots can be varied as well. Subsequently, by loading the proposed SECSRR into the conventional HMSIW, the HMSIW-SECSRR unit cell is formed. Fig. 2 sketches the derivation process from conventional HMSIW-CSRR unit cell to three different HMSIW-SECSRR unit cells. Firstly, to generate the evanescent mode resonance more easily, the splits of CSRR and SECSRRs are supposed to be close to the open side of HMSIW. Secondly, for the HMSIW-CSRR and HMSIW-SECSRR unit cells in Fig. 2, z-axis is the transmission direction, which is just parallel to the metallized-vias row, while x-axis is the transverse standing-wave direction, which is perpendicular to the row of metallized-vias.

As shown in Fig. 2, for Type-I HMSIW-SECSRR unit cell, all stub slots are with the same width and length, while numbers of the stub slots along z- and x-axes are different. Meanwhile, for Type-II and Type-III HMSIW-SECSRR unit cells, lengths and numbers of the stub slots along z-axis are respectively different from the corresponding counterparts along x-axis. More exactly, for all the three HMSIW-SECSRR unit cells, there are ten stub slots on each side which are perpendicular to the transmission direction (namely these stub slots are along z-axis). Meanwhile, there are nine stub slots embedded on the close-to-via side in each SECSRR, whereas the number of stub slots embedded on the split side is eight (namely these stub slots are along x-axis). Furthermore, in Type-II unit cell, stub slots along z-axis are longer than those along x-axis. For Type-III case, stub slots along z-axis are shorter. Therefore, Type-II and Type-III HMSIW-SECSRR unit cells can exhibit more design flexibility than the conventional and Type-I ones.

Thereafter, the simplified equivalent circuit models of the conventional HMSIW-CSRR and proposed HMSIW-SECSRR unit cells are given in Fig. 2 as well. The CSRR can be modeled as a parallel resonant network composed of a capacitor with capacitance C_{r0} and an inductor with inductance L_{r0}. Then, for the three proposed SECSRRs, L_{ri} and C_{ri} denote their corresponding equivalent inductance and capacitance, respectively, where $i = 1$ for Type I, $i = 2$ for Type-II, and $i = 3$ for Type-III. As

CSRR is changed into SECSRR, L_{r0} will change to L_{ri}, and C_{r0} will change to C_{ri}. Moreover, there is a certain relationship between them as below:

$$L_{ri} = L_{r0} + L_{si}, \quad (i = 1, 2, 3) \tag{1}$$

$$C_{ri} = C_{r0} + C_{si}, \quad (i = 1, 2, 3) \tag{2}$$

where L_{si} and C_{si} represent the inductance and capacitance contributed from the embedded stub slots in the three proposed SECSRRs.

Moreover, the resonant frequency of the SECSRRs can be expressed as:

$$f_{ri} = \frac{1}{2\pi\sqrt{L_{ri}C_{ri}}}, \quad (i = 1, 2, 3) \tag{3}$$

Afterwards, to realize the operation principles of the proposed HMSIW-SECSRR unit cell more clearly and deeply, it is essential to investigate their resonance properties. Thus, some eigenmode analyses are carried out by using a commercial full-wave simulator based on the finite element method. In the simulation setup, the substrate has a fixed thickness of 1.0 mm, a stable relative permittivity of 4.4, and a fixed dielectric loss tangent of 0.005. Table 1 gives the simulated electric fields magnitude distributions of the lower six eigenmodes of the conventional HMSIW, HMSIW-CSRR, and the proposed HMSIW-SECSRR unit cells, as well as their geometrical topologies with physical dimensions for simulations. It can be easily obtained from Table 1 that the conventional HMSIW unit cell has a dominant eigenmode of 3.43 GHz with an unloaded quality factor (Q_u) of 315.3. Moreover, all of its higher-order eigenmodes operate over 7.7 GHz, with unloaded quality factors larger than 377.3. Then, as a CSRR is loaded into the conventional HMSIW unit cell, the dominant eigenmode will operate at 1.21 GHz, which is much lower than that of HMSIW. Meanwhile, the associated Q_u decreases to 131.9 as well, which is mainly attributed to the radiation loss effect caused by defected CSRR. For the conventional HMSIW-CSRR unit cell, all of its second, third, fourth and fifth eigenmodes resonate in the frequency range of 5–8 GHz. Hence, in the frequency region close to the dominant eigenmode, the resonance properties of the HMSIW-CSRR unit cell are much more complex than that of the conventional HMSIW one. Obviously, the resonance eigenmodes of HMSIW-CSRR are much different from those of HMSIW, which will make their potential applications different as well. Later, for the proposed Type-I HMSIW-SECSRR unit cell, it can be easily captured that, by embedding the stub slots into the HMSIW-CSRR, the dominant eigenmode resonant frequency decreases effectively from 1.21 GHz to 1.04 GHz, while Q_u only changes a bit, decreasing from 131.9 to 127.3. Meanwhile, the other five higher-order eigenmodes of Type-I unit cell operate between 4.47 GHz and 6.56 GHz, and the corresponding unloaded quality factors for these five higher-order eigenmodes are between 239.8 and 300.7. Moreover, for Type-II HMSIW-SECSRR unit cell, its dominant eigenmode resonates at 1.03 GHz with a Q_u of 132.7, and its electric field distribution is similar to that of Type-I unit cell, whereas their second eigenmodes are quite different from each other, as well as their third eigenmodes, which can be easily summarized from their electric filed distributions. More exactly, Type-II unit cell is with a second eigenmode resonant frequency of 3.92 GHz, much lower than that of Type-I unit cell. Finally, the proposed Type-III HMSIW-SECSRR unit cell has the lowest dominant eigenmode frequency of 0.99 GHz, as well as the lowest Q_u of 126.7. Its second eigenmode resonates at a similar frequency of the second-order eigenmode of Type-II unit cell, while their electrical-field distributions are quite differently. Moreover, as shown in Table 1, their corresponding third-, fourth- and fifth-order eigenmodes are with similar electrical-field distributions.

Moreover, several further investigations should be further delivered on the transmission properties of the proposed HMSIW-SECSRR unit cells. These numerical simulations are carried out by using the same aforementioned full-wave software, and the substrate is set with some fixed parameters for the convenience of comparison as well. The substrate thickness is 1.016 mm; the relative permittivity is 4.38; the relative permeability is 1; the loss tangent is 0.005; and the cover metal is conventional lossy copper with a thickness of 0.035 mm. Fig. 3 shows simulated magnitude of transmission coefficient ($|S_{21}|$) of the proposed HMSIW-SECSRR unit cells versus different varied parameters. In Fig. 3(a), influence from the number of stub slots on the transmission properties is studied, with other geometrical parameters for simulation being given in the inset. Here, *Nx* denotes the number of stub slots along x-axis, and *Nz* represents the stub slots along z-axis. All the stub slots on each side of CSRR are set with identical width and length. Hence, this case is the very Type-I HMSIW-SECSRR unit cell. It can be easily

Table 1. Electric-field distributions of the lower six eigenmodes of HMSIW, HMSIW-CSRR and HMSIW-SECSRR unit cells.

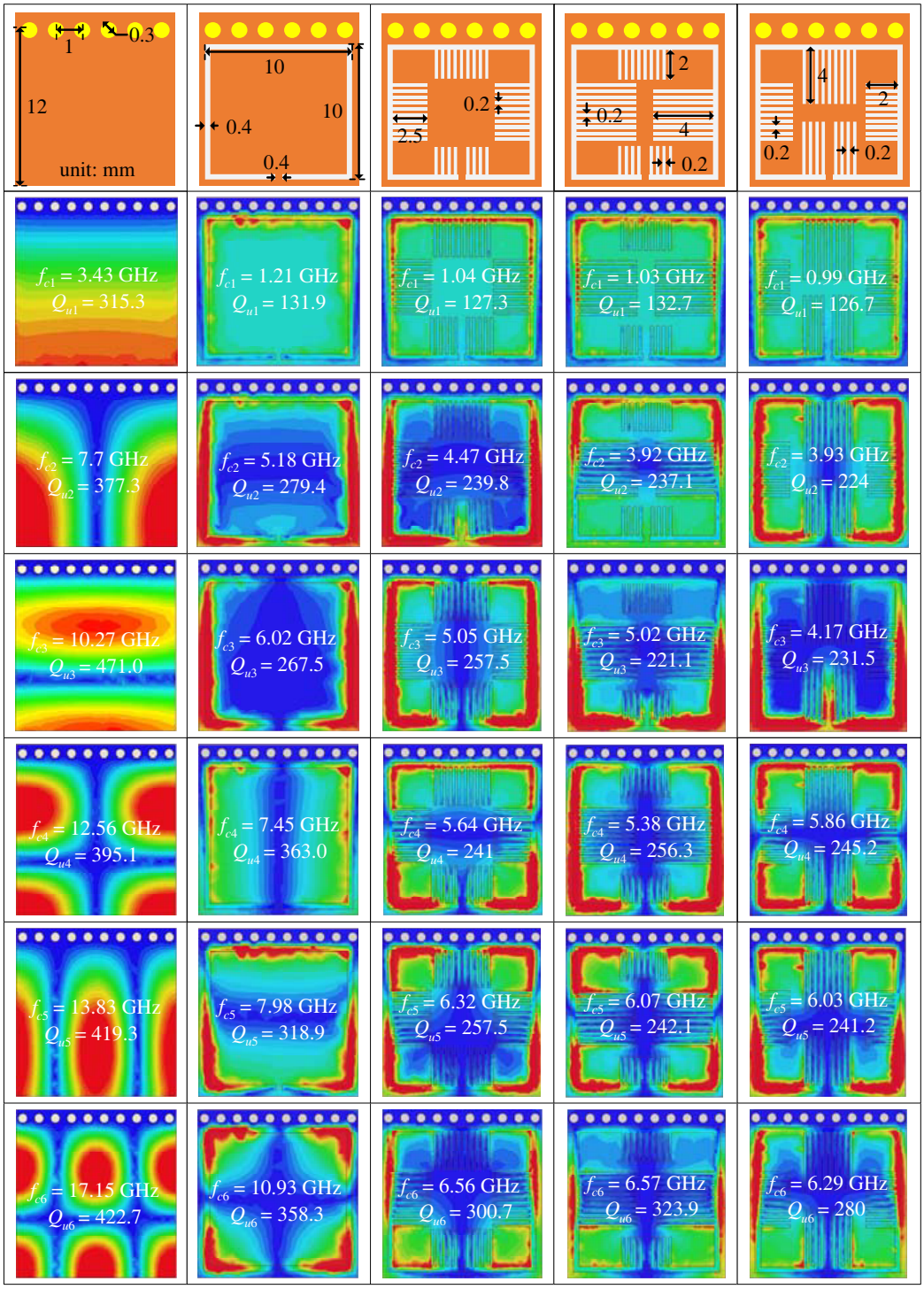

obtained that the resonant frequency decreases from 1.18 GHz to 1.1 GHz as Nx increases from 1 to 13, and Nz increases from 2 to 14. Meanwhile, the transmission zero located at the higher stopband also shifts downwards from 2.26 GHz to 2 GHz, which makes the selectivity of Type-I unit cell better. Then, for Fig. 3(b), it is also for the Type-I case. Here, numbers of the stub slots are $Nx = 9$ and $Nz = 10$, and

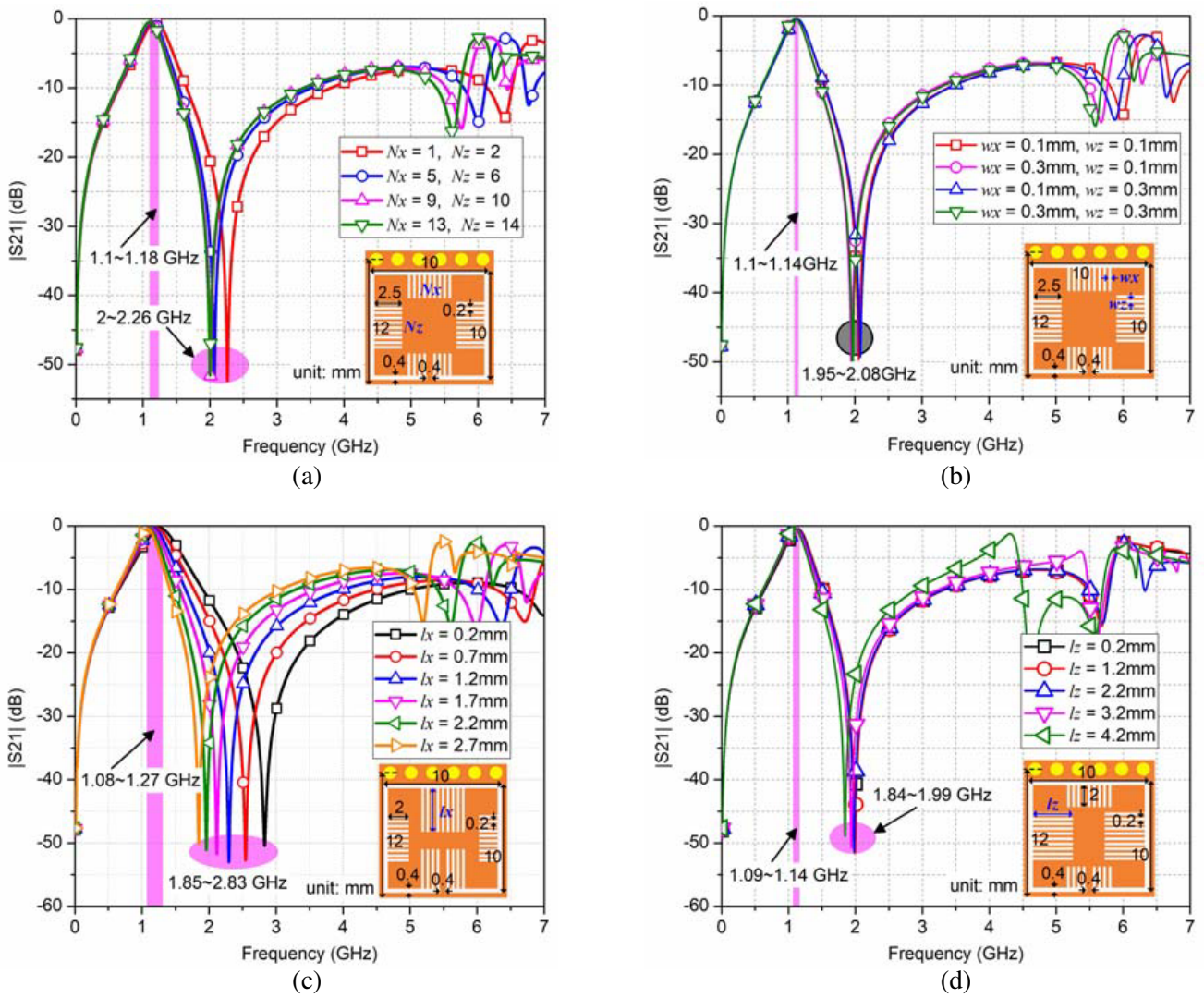

Figure 3. Simulated $|S_{21}|$ of HMSIW-SECSRR unit cells versus varied parameters. (a) Number of stub slots; (b) widths of stub slots; (c) length of stub slots along x-axis; (d)length of stub slots along z-axis.

all stub slots are with the same length of 2.5 mm. As shown in Fig. 3(b), with widths of the stub slots wx and wz jittering from 0.1 mm to 0.3 mm, the resonant frequency changes from 1.14 GHz to 1.1 GHz; transmission zero's location shifts from 2.08 GHz to 1.95 GHz; and the spurious passband moves from 6.3 GHz to 6 GHz. Therefore, it can be summarized that the widths of stub slots only have very slight influence on the transmission coefficients of Type-I HMSIW-SECSRR unit cell.

Subsequently, for Type-II and Type-III HMSIW-SECSRR unit cells, the situation will be much different. Firstly, in Fig. 3(c), the stub slots along x-axis are with a fixed length and width of 2 mm and 0.2 mm, respectively, while the stub slots along z-axis are with a fixed width of 0.2 mm but varied length lz. Hence, for this case, it is the very Type-II HMSIW-SECSRR unit cell. According to Fig. 3(c), as lz varies from 0.2 mm to 4.2 mm, the unit cell's resonant frequency shifts downwards from 1.14 GHz to 1.09 GHz, and the transmission zero's location moves from 1.99 GHz to 1.88 GHz. Therefore, even though lz enlarges heavily, the transmission coefficient only changes a little. Moreover, there is another interesting phenomenon. As lz changes between 0.2 mm and 3.2 mm, the transmission coefficient is quite stable, with only the resonant frequency and transmission zero's location swinging slowly and slightly, and the spurious passband existing at 6 GHz. However, as lz lengthens to 4.2 mm, the resonant frequency

and transmission zero's location will both move downwards notably. Meanwhile, another extra parasitic passband will occur near 4.3 GHz. Hence, large lz might change the resonance characteristics of Type-II HMSIW-SECSRR unit cell. Then, for Fig. 3(d), the stub slots along z-axis are with fixed length of 2 mm and fixed width of 0.2 mm, while the stub slots along x-axis are with varied length lx, namely it is the very Type-III HMSIW-SECSRR unit cell case. According to Fig. 3(d), as lx enhances from 0.2 mm to 2.7 mm, the resonant frequency moves from 1.27 GHz to 1.08 GHz; the transmission zero's location shifts lower from 2.83 GHz to 1.85 GHz; and the spurious passband changes from 7 GHz to 5.5 GHz. Obviously, with the stub slots along x-axis increasing longer, selectivity of the Type-III unit cell also becomes better.

2.2. Machining Tolerance Sensitivity

As known, in many microwave and millimeter wave applications, the accuracy and consistency between simulation design and fabrication realization is extremely important for the high-performance operation of the entire system. That is to say, for typical resonators and bandpass filters, the resonant frequency, transmission zero's location, selectivity, and out-of-band rejection should keep steady between simulation and fabrication. Unfortunately, in practical applications, the fabrication process usually brings in unpredictable and unexpected imprecision to the components prototypes due to the inherent fabrication tolerance, which influences the application practicability heavily. Currently, there are two main kinds of PCB fabrication processes. One is chemical processing, and the other is machining chiseling. For the multilayer PCB fabrication, chemical processing is more preferred owing to its high precision. However, it is more complex than the machining chiseling method as well. Therefore, for single layer PCB fabrication, machining chiseling is much more preferred. Nevertheless, the precision of machining chiseling is generally much worse than that of chemical processing. Hence, in the practical design of components and circuits with machining chiseling, it is significantly essential to demonstrate the fabrication tolerance sensitivity of the components.

To evaluate the machining tolerance sensitivity of proposed HMSIW-SECSRR unit cells, some numerical simulations are implemented. To simplify the analyses process, the same full-wave simulator and substrate setup as mentioned in Subsection 2.2 are utilized. The DNC-330D from DM Machinery is a typical drilling machine for PCB etching. Its minimum drilling bit is with a diameter of 0.2 mm, and the typical fabrication tolerance is ±10%. Namely, the minimum drilling bit can chisel a slot with a size of 0.18–0.22 mm. Hence, in the machining tolerance sensitivity simulations, all related geometrical parameters are supposed to be evaluated within such drilling and chiseling imprecision. The simulated $|S_{21}|$ with machining tolerance sensitivity of the conventional HMSIW-CSRR and proposed HMSIW-SECSRR unit cells are given in Fig. 4. As shown in the inset of Fig. 4(a), the CSRR is set with side lengths of $x1 = 10 \pm 0.1$ mm and $x2 = 10 \pm 0.1$ mm. Moreover, the CSRR is with a width of $y1 = 0.4 \pm 0.04$ mm, and the split is with a width of $lc = 0.4 \pm 0.04$ mm. Then, it can be obtained from Fig. 4(a) that resonant frequency of the conventional HMSIW-CSRR unit cell jitters between 1.14 and 1.34 GHz, corresponding to a fractional frequency offset of ±8.11% with the center of 1.24 GHz. Meanwhile, the transmission zero's location swings from 2.71 GHz to 2.94 GHz. Subsequently, for the Type-I HMSIW-SECSRR unit cell in Fig. 4(b), $x1 = x2 = 10 \pm 0.1$ mm, $y1 = 0.4 \pm 0.04$ mm, and $lc = 0.4 \pm 0.04$ mm. Meanwhile, the stub slots are with length of $lx = 2.5 \pm 0.1$ mm and width of $wx = 0.2 \pm 0.02$ mm. According to Fig. 4(b), the resonant frequency swings between 1.03 GHz and 1.17 GHz, corresponding to a fractional frequency offset of ±6.36% with the center of 1.1 GHz. Moreover, location of the transmission zero changes in the range of 1.77–2.03 GHz. Later, in Fig. 4(c), $x1 = x2 = 10 \pm 0.1$ mm, $y1 = 0.4 \pm 0.04$ mm, $lc = 0.4 \pm 0.04$ mm, $lx = 1.8 \pm 0.1$ mm, $lz = 4.2 \pm 0.1$ mm, $wx = wz = 0.2 \pm 0.02$ mm. With these simulated tolerances, resonant frequency of Type-II HMSIW-SECSRR unit cell covers 1.03–1.15 GHz, and the transmission zero's location ranges from 1.75 GHz to 1.99 GHz. Thereby, for this case, the resonant frequency has a changeable range of ±5.50%, and the center of resonant frequency is 1.09 GHz. Finally, for the Type-III unit cell in Fig. 4(d), the machining tolerances for simulations are set as follows: $x1 = x2 = 10 \pm 0.1$ mm, $y1 = 0.4 \pm 0.04$ mm, $lc = 0.4 \pm 0.04$ mm, $lx = 4.2 \pm 0.1$ mm, $lz = 1.8 \pm 0.1$ mm, $wx = wz = 0.2 \pm 0.02$ mm. It can be captured from Fig. 4(d) that the resonant frequency can jitter over 0.96–1.06 GHz, while the transmission zero's location swings near 1.50–1.72 GHz. Hence, the resonant frequency is centered at 1.01 GHz, with a relative offset of ±4.95%. Therefore, by comparing the fractional frequency offset of the conventional

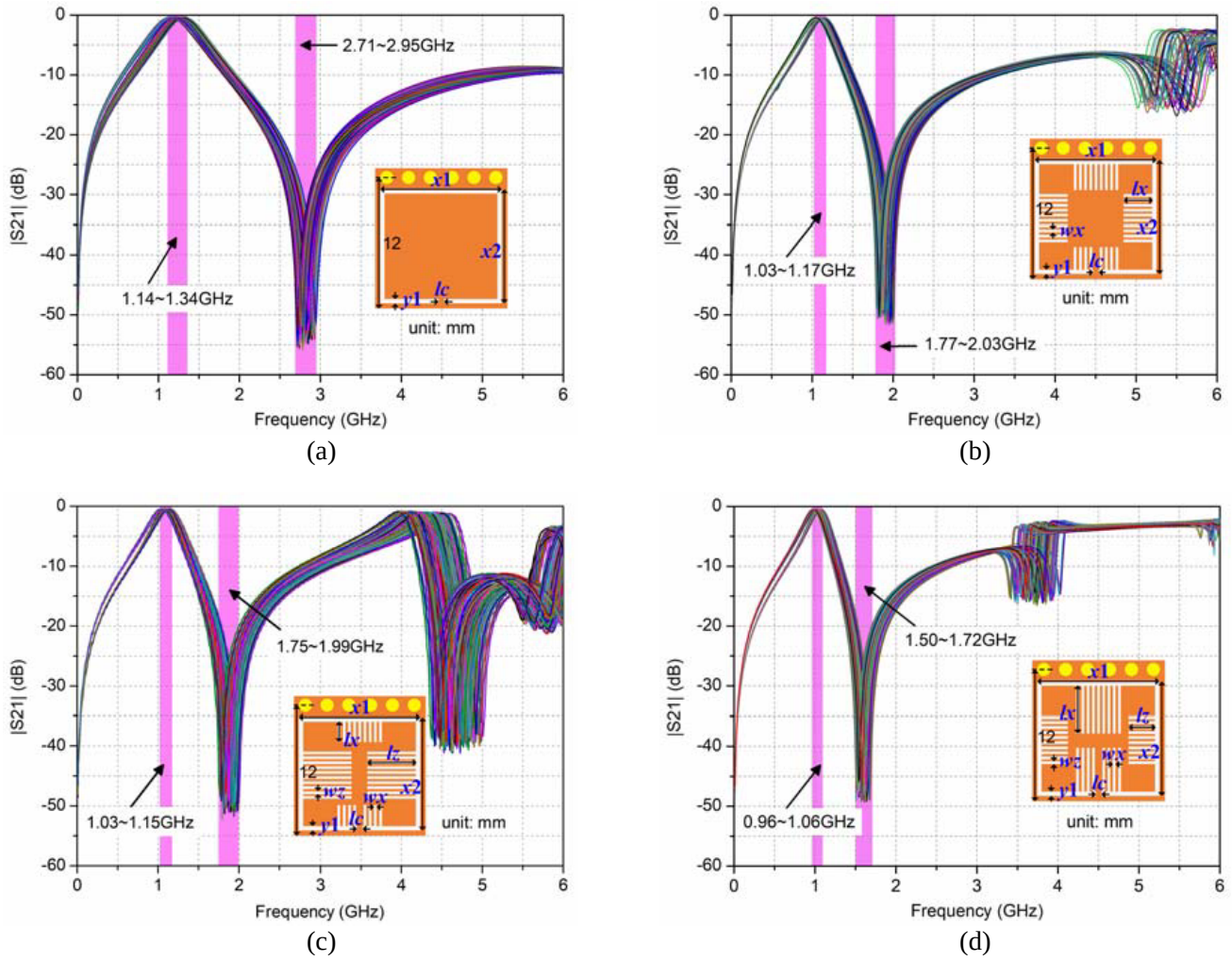

Figure 4. Simulated machining tolerance sensitivities of various unit cells. (a) HMSIW-CSRR; (b) Type-I HMSIW-SECSRR; (c) Type-II HMSIW-SECSRR; (d) Type-III HMSIW-SECSRR.

HMSIW-CSRR and proposed HMSIW-SECSRR unit cells, it can be found that all the three proposed unit cells can achieve smaller frequency offset, and Type-III unit cell is able to exhibit the best frequency offset performance. Hence, all the three proposed HMSIW-SECSRR unit cells have smaller machining tolerance sensitivity than HMSIW-CSRR, while Type-III occupies the smallest value. In other words, by embedding the stub slots into HMSIW-CSRR, machining tolerance sensitivity of the entire unit cell can be decreased effectively, which indicates that the proposed unit cells are much more preferred and demanded for practical microwave circuits and components applications.

Additionally, it is worth mentioning that the four unit cells in Fig. 4 are quite different from each other. As shown in Fig. 4(a), the conventional HMSIW-CSRR exhibits only one passband below 6 GHz. In Fig. 4(b), Type-I HMSIW-SECSRR can exhibit a spurious passband around 5.5 GHz. Then, according to Figs. 4(c) and 4(d), Type-II HMSIW-SECSRR has a spurious passband between 4 and 4.7 GHz, whereas Type-III HMSIW-SECSRR shows a spurious passband near 3.5–4.0 GHz. Moreover, the spurious passband of Type-III unit cell is wider but weaker, while the spurious passband of Type-II unit cell is narrower but stronger. From this viewpoint, Type-III unit cell is more suitable for specific applications than Type-II one since it is more easily to suppress the spurious passband.

3. HMSIW-SECSRR FILTERS DESIGN

To verify the availability and effectiveness of the proposed HMSIW-SECSRR unit cells, evanescent-mode filters are designed. Firstly, the proposed unit cells are utilized to design single-pole evanescent-mode filters to verify their availability. As depicted in Fig. 4, Type-II and Type-III unit cells show similar transmission properties, while Type-III one exhibits weaker spurious performance. Hence, for the convenience of comparison, both Type-I and Type-III unit cells are utilized to design single-pole evanescent-mode filter. Fig. 5 sketches detailed configuration of the proposed Type-I and Type-III single-pole evanescent-mode filters. It can be easily captured that the proposed Type-I single-pole filter mainly consists of a Type-I HMSIW-SECSRR unit cell in the center and two 50-ohm microstrip transmission lines at the input and output (I/O) ports. The direct microstrip-HMSIW transitions are utilized to connect Type-I unit cell and 50-ohm microstrip lines, which can also contribute to the compactness of the entire single-pole filter. Similarly, as shown in Fig. 7(b), the proposed Type-III single-pole filter is mainly made of Type-III HMSIW-SECSRR with longer stub slots along x-axis, 50-ohm microstrip lines, and direct transitions. For both single-pole filters, there is no inner coupling between adjacent resonators. Hence, the operation bandwidths, insertion losses, and return losses are mainly controlled by their external quality factors. As depicted in [4], the external quality factor of coupled-resonator filter is typically determined by the feeding method. Here, for the two single-pole cases, the external quality factors are mainly determined by two parts: one is the feeding microstrip, and the other is the metal width between the edge of HMSIW and the SECSRR. Generally, as the metal between HMSIW's edge and SECSRR becomes wider, the external quality factor will become larger, and the bandwidth will become narrower. Meanwhile, as the feeding microstrip shifts close to the metallic vias, i.e., far away from the open side of HMSIW, the external quality factor will get larger, and the bandwidth will get narrower. Additionally, the shape of microstrip-HMSIW transitions can influence the filters' overall performance as well. Fortunately, since the microstrip-HMSIW transitions have been fixed in direct form, the design and study on external quality factor can be simpler.

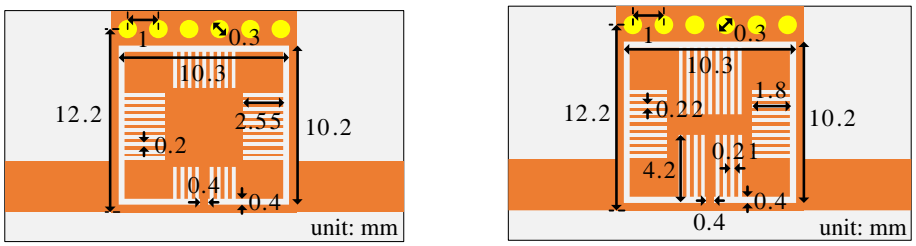

Figure 5. Configuration and optimized dimensions of the single-pole evanescent-mode HMSIW-SECSRR filters: (a) Type-I; (b) Type-III.

Afterwards, the Kappa438 laminate material with a thickness of 1.016 mm is utilized to design the proposed single-pole filters. Kappa438 is an emerging glass reinforced hydrocarbon resin material with low cost and compatibility with conventional epoxy FR-4 process. It is with a relative permittivity of 4.38, which is extremely close to that of conventional FR-4 series substrate, while its dielectric loss tangent is only 0.005, only a quarter of that of FR-4. Hence, the Kappa438 is actually an ultra-fit alternative of conventional FR-4 substrate. Then, both single-pole evanescent-mode filters in Fig. 5 are separately modeled and simulated by using the same commercial simulator mentioned above. During the optimization of filters' dimensions, the parameter sweeping approach is utilized owing to its fast convergence with manual intervention, instead of the default automatic parameter tuning that might cost much more time. All optimized dimensions of the proposed single-pole HMSIW-SECSRR filters are listed in Fig. 5 as well.

Later, to further improve the performance of evanescent-mode filters, a two-pole filter is developed with Type-III HMSIW-SECSRR unit cell, with its detailed configuration given in Fig. 6. The two-pole filter mainly consists of two Type-III unit cells, two 50-ohm microstrip lines, two direct HMSIW-

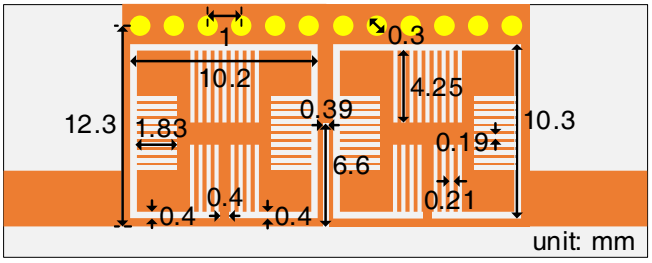

Figure 6. Configuration and optimized dimensions of the Type-III two-pole HMSIW-SECSRR filter.

microstrip transitions, and a mixed coupling section. The mixed coupling section contains an HMSIW section and a slot from the open edge. Therefore, with the capacitance effect contributed from the slot and the inductance effect generated by the HMSIW section, the mixed electrical-magnetic cross coupling can be produced, thus to generate an extra transmission zero to the proposed two-pole filter. Therefore, the HMSIW-slot coupling structure is quite simple and useful for the filter design.

It is well known that the coupled-resonator filter design generally starts from the synthesis of initial prototyped filter. Hence, for this case, the initial Type-III HMSIW-SECSRR filter is designed with a center frequency (f_c) of 8.6 GHz, a fractional bandwidth (FBW) of 12%, and an in-band insertion loss ripple of 0.1 dB. Then, the initiated inner coupling coefficients (ki) and external quality factor (Q_e) of the proposed initial filter can be calculated by using the elements of the Chebyshev lowpass prototype filter. For this case, since the filter only contains two cascaded resonators, the coupling coefficients matrix $\mathbf{k}$ and external quality factor Q_e can be initially calculated as:

$$\mathbf{k} = \begin{bmatrix} 0 & 0.1657 \\ 0.1657 & 0 \end{bmatrix} \tag{4}$$

$$Q_e = 7.025 \tag{5}$$

Thereafter, ki and Q_e of the proposed two-pole evanescent-mode filter are supposed to be numerically studied. The related simulations are delivered by using the same aforementioned full-wave simulator separately under eigen-mode and driven-mode conditions. Fig. 7(a) shows the relation between ki and several geometrical parameters, as well as the model with other fixed geometrical dimensions for simulation. Obviously, as the slot length lp becomes longer, the coupling coefficient ki decreases. Meanwhile, as the slot width wp gets larger, ki decreases a bit as well. Moreover, as the spacing between SECSRR and HMSIW's open edge cp enlarges, the coupling coefficient will enlarge. Hence, in the filter design, the coupling strength and bandwidth can be tuned flexibly and easily by these geometrical parameters. Meanwhile, Fig. 7(b) gives the simulated Q_e with several significant geometrical parameters at the feeding point. Other fixed dimensions are shown in the inset. According to Fig. 7(b), as the spacing between the feeding line and the open edge of HMSIW $p1$ gets longer, Q_e becomes larger. As the spacing between the split of CSRR and the open edge of HMSIW cp widens, Q_e will get smaller a bit. Moreover, as the width of edge metal $s1$ becomes larger, Q_e will enlarge notably.

Furthermore, by taking Fig. 7 with the synthesized coupling coefficients in Eq. (4) and the external quality factor in Eq. (5) into consideration, the initiated geometrical parameters of the proposed SW-SIW cavity filters can be selected. The entire two-pole evanescent-mode filter in Fig. 6 is later carefully modeled, simulated, and optimized in the commercial simulator. During the numerical optimization, the artificial tuning strategy is applied. Firstly, the initial values of geometrical parameters obtained from eigenmode and coupling analyses are set as the mid-values. Secondly, two values for each geometrical parameter, one larger than the mid-value and the other smaller, are selected. Thirdly, by simulating the proposed filters with different geometrical dimensions, different scattering parameters can be captured, and influence trends from geometrical dimensions on the scattering parameters can be easily summarized. With such changing trends, it will be much faster to capture the optimized values of geometrical parameters for the filters. After sufficient simulations, the optimized geometrical parameters are given in Fig. 6 as well.

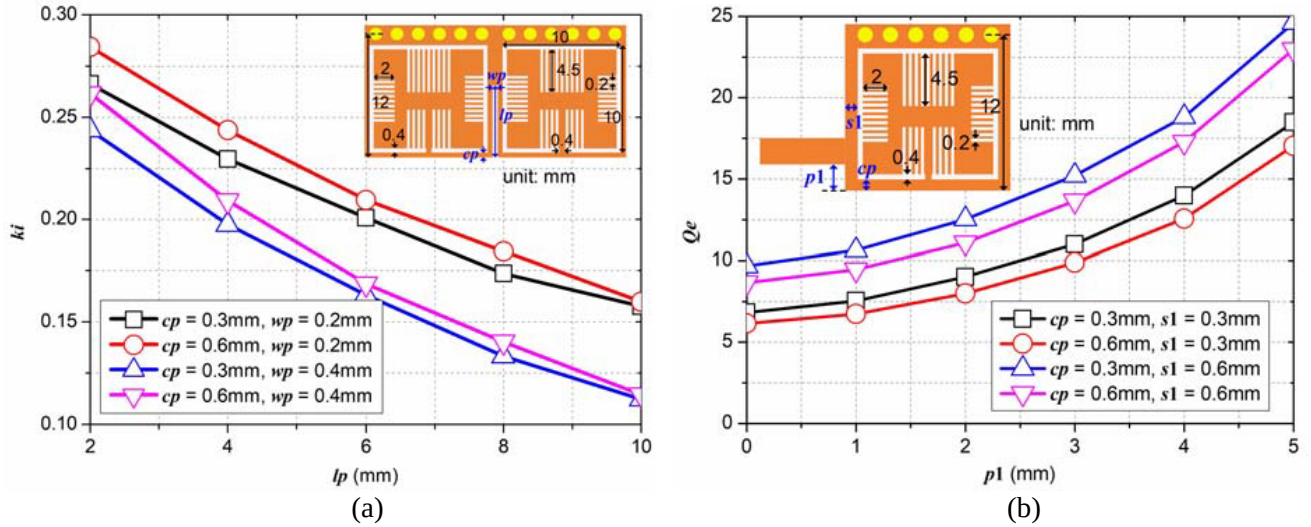

(a) (b)

Figure 7. Simulated coupling coefficients (ki) and external quality factors (Q_e) of Type-III HMSIW-SECSRR unit cell: (a) ki, and (b) Q_e.

4. EXPERIMENTS AND DISCUSSIONS

By using the standard machining process, the proposed single-pole and two-pole evanescent-mode filters are chiseled on a Kappa438 substrate with a thickness of 1.016 mm, a relative permittivity of 4.38 ± 0.02, and a loss tangent of 0.005. Photographs of the three fabricated evanescent-mode HMSIW-SECSRR filters are shown in the insets of Fig. 8, with their measured results captured by a Keysight N5220A vector network analyzer, as well as the simulations. As shown in Fig. 8(a), the fabricated single-pole Type-I filter achieves a center frequency of 0.905 GHz and a bandwidth of 130 MHz, corresponding to an FBW of 11.76%. Its minimum in-band insertion loss is 0.51 dB, and the return loss is better than 15 dB. Meanwhile, a transmission zero with rejection over 50 dBc is generated at 1.5 GHz. For the single-pole Type-III filter in Fig. 8(b), the center frequency is about 0.85 GHz, the bandwidth 120 MHz, the insertion loss 0.52 dB, and the return loss over 13.5 dB. A transmission zero at 1.32 GHz is achieved as well, with an out-of-band rejection near 50 dBc. Moreover, for the fabricated two-pole Type-III filter in Fig. 8(c), it exhibits a center frequency about 0.861 GHz and a bandwidth of 100 MHz, corresponding to an FBW of 11.63%, which is only a bit different from the design values. Meanwhile, its in-band insertion loss is 0.96 dB, and its return loss is better than 20 dB. Two transmission zeros located at 1.25 GHz and 1.35 GHz are produced as well. The lower transmission zero brings in an out-of-band rejection of 57 dBc, while the upper one shows 58 dBc rejection performance.

Above all, it can be obtained from Fig. 8 that the measured results of all the three fabricated filters are in excellent agreement respectively with their corresponding simulations, not only in the operation passband, but also in the out of band. Hence, the good consistency between simulations and measurements has further demonstrated that the proposed HMSIW-SECSRR unit cells can exhibit lower machining tolerance sensitivity than the conventional HMSIW-CSRR. Therefore, embedding stub slots is a promising method to decrease the fabrication tolerance sensitivity of specific microwave components.

Table 2 summarizes the comparison between the proposed filters and some reported works using similar technologies. To make the comparison reasonable and convincing, only the reported filters integrated with SIW and CSRR-like defected structures are considered. In [8], the open CSRR (OCSRR) is loaded into a SIW section to constitute a SIW-OCSRR resonator. The stepped-impedance resonator (SIR) technique is introduced into SIW-CSRR filters design in [9]. A modified CSRR (MCSRR) is proposed in [10] by inner extending the split in menderline shape for HMSIW filter implementation. Moreover, the fractal open CSRR (FOCSRR) and G-shaped resonator (CGR) are presented in [11] and [12] to reduce the circuitry physical sizes, respectively. Firstly, it can be easily obtained that

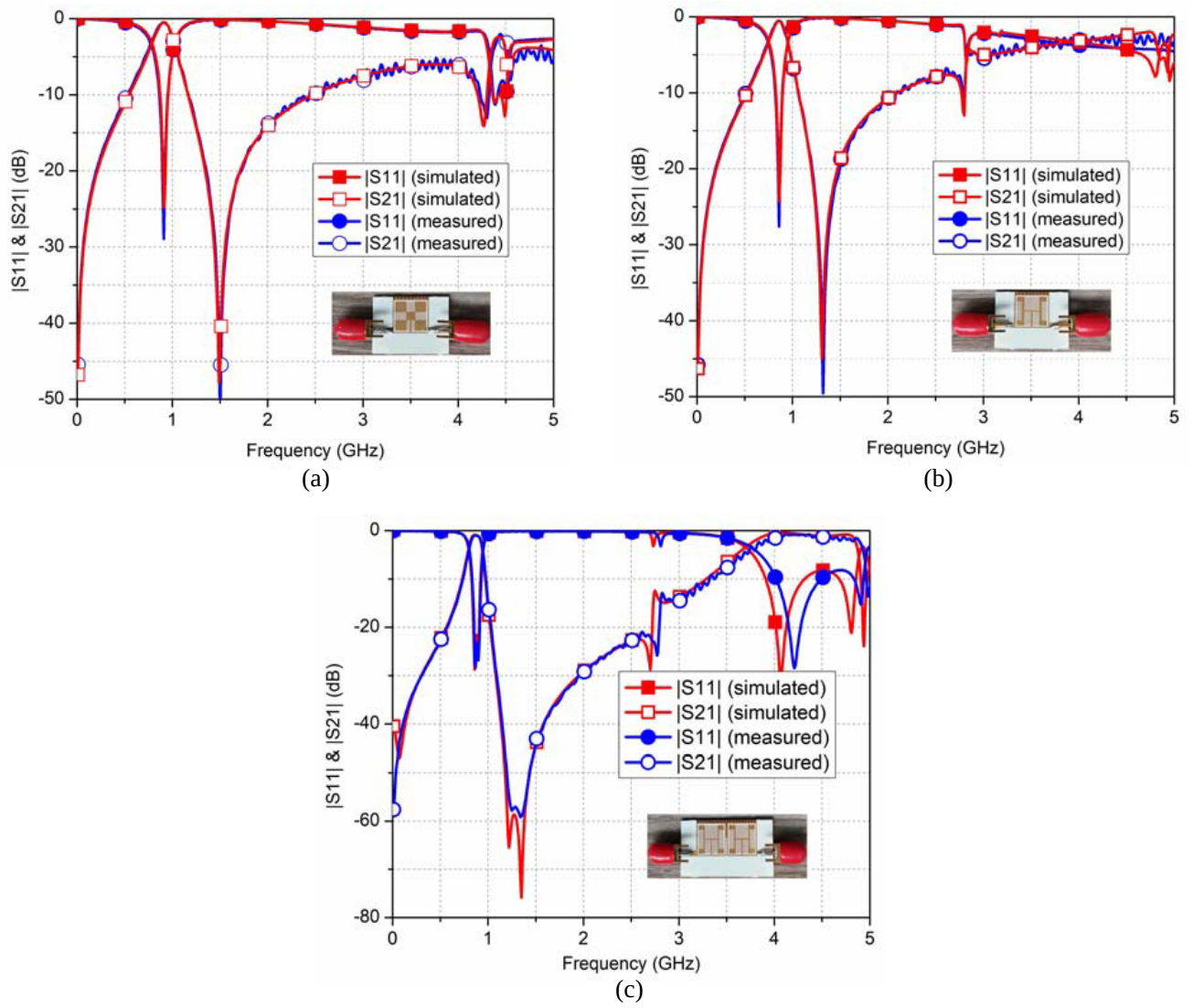

Figure 8. Simulated and measured results of the fabricated HMSIW-SECSRR filters. (a) Single-pole Type-I; (b) single-pole Type-III; (c) two-pole Type-III.

Table 2. Comparison between the proposed filters and some reported similar works.

Ref.	Topology	Poles	f_c (GHz)	FBW	Insertion loss (dB)	Return loss (dB)	Size ($\lambda_0^2/\varepsilon_r$)	Reduced fabrication tolerance sensitivity
[8]	SIW-OCSRR	1	5.5	9.7%	1.5	10	0.04988	No
[9]	SIW-SIRCSRR	2	1.58	9.4%	2	> 14	0.02610	No
[10]	HMSIW-MCSRR	2	2.4	$> 10\%$	1.45	16	0.01898	No
[11]	SIW-FOCSRR	2	2.4	12.5%	2.2	21	0.04254	No
[12]	SIW-CGR	2	1.82	7.8%	1.1	21	0.01447	No
Type-I	HMSIW-SECSRR	1	0.905	11.76%	0.51	15	0.00603	Yes
Type-III	HMSIW-SECSRR	1	0.85	14.12%	0.52	13.5	0.00532	Yes
Type-III	HMSIW-SECSRR	2	0.861	11.63%	0.96	20	0.01118	Yes

compared with all the reported filters in Table 2, the proposed HMSIW-SECSRR filters are with the smallest relative electrical size and smallest insertion loss, as well as reduced fabrication tolerance sensitivity. Although the works in [8, 10, 11] are with much higher center frequencies that might increase the insertion loss, the proposed filters are still with attractive performance. Actually, according to the datasheet released by Angels Electronics, the SMA connector can contribute to the insertion loss with a value of $0.06 \cdot f^{0.5}$ dB, where f is in GHz. Hence, as the proposed one-pole and two-pole Type-III HMSIW-SECSRR filters are redesigned with a center frequency around 5.5 GHz, its insertion loss would be $0.52 + 0.141 = 0.661$ dB and $0.96 + 0.141 = 1.101$ dB, respectively, which is still much lower than that in [8, 10, 11]. Moreover, the proposed HMSIW-SECSRR filters also achieve similar return loss performance to those in [8–10], only worse than those in [11, 12]. Hence, in a word, the proposed filters exhibit good insertion loss, compact size, and reduced fabrication tolerance sensitivity, which indicates promising practicability for RF and microwave applications.

5. CONCLUSION

This work presents single-pole and two-pole evanescent-mode HMSIW-SECSRR filters. The proposed SECSRR composed of stub slots of various lengths can help to enhance the equivalent capacitance and inductance of CSRR, so that to realize size miniaturization. More importantly, by introducing stub slots into conventional CSRR, machining tolerance sensitivities of the HMSIW-SECSRR unit cells have been reduced effectively, and the resonance frequency offset resulting from machining tolerance has been squeezed notably. Based on numerical and experimental results, the proposed filters are with smaller sizes and better stabilities on center frequency, selectivity, and out-of-band performance, which is suitable for RF and microwave circuits, components, and system applications.

ACKNOWLEDGMENT

This work is supported by Sichuan Science and Technology Program under grants 2020YFG0447 and 2021YFG0337.

REFERENCES

1. Deslandes, D. and K. Wu, "Integrated microstrip and rectangular waveguide in planar form," *IEEE Microwave and Wireless Components Letters*, Vol. 11, No. 2, 333–335, Feb. 2001.
2. Hong, W., B. Liu, Y. Wang, Q. Lai, et al., "Half mode substrate integrated waveguide: A new guided wave structure for microwave and millimeter wave application," *2006 Joint 31st International Conference on Infrared Millimeter Waves and 14th International Conference on Terahertz Electronics*, 219, Shanghai, China, 2006.
3. Zhai, G., W. Hong, K. Wu, J. Chen, et al., "Folded half mode substrate integrated waveguide 3 dB coupler," *IEEE Microwave and Wireless Components Letters*, Vol. 18, No. 8, 512–514, Aug. 2008.
4. Dong, Y., T. Yang, and T. Itoh, "Substrate integrated waveguide loaded by complementary split-ring resonators and its applications to miniaturized waveguide filters," *IEEE Transactions on Microwave Theory and Techniques*, Vol. 57, No. 9, 2211–2223, Sep. 2009.
5. Zhang, Q., W. Yin, S. He, et al., "Compact substrate integrated waveguide (SIW) bandpass filter with complementary split-ring resonators (CSRRs)," *IEEE Microwave and Wireless Components Letters*, Vol. 20, No. 8, 426–428, Aug. 2010.
6. Kang, H. and S. Lim, "Electrically small dual-band reconfigurable complementary split-ring resonator (CSRR)-loaded eighth-mode substrate integrated waveguide (EMSIW) antenna," *IEEE Transactions on Antennas and Propagation*, Vol. 62, No. 5, 2368–2373, May 2014.
7. Pradhan, N., K. Subramanian, and R. Barik, "Design of compact substrate integrated waveguide based triple- and quad-band power dividers," *IEEE Microwave and Wireless Components Letters*, Vol. 31, No. 4, 365–368, Apr. 2021.

8. Danaeian, M., K. Afrooz, A. Hakimi, and A. R. Moznebi, "Compact bandpass filter based on siw loaded by open complementary split-ring resonators," *International Journal of RF and Microwave Computer-Aided Engineering*, Vol. 26, No. 8, 674–682, Aug. 2016.
9. Danaeian, M., K. Afrooz, and A. Hakimi, "Miniaturization of substrate integrated waveguide filters using novel compact metamaterial unit-cells based on sir technique," *AEU — International Journal of Electronics and Communications*, Vol. 84, 62–73, Feb. 2018.
10. Danaeian, M., R. Moznebi, and K. Afrooz, "A novel super compact half-mode substrate-integrated waveguide filter using modified complementary split-ring resonator," *International Journal of RF and Microwave Computer-Aided Engineering*, Vol. 29, No. 6, 21709, 1–8, Feb. 2019.
11. Danaeian, M. and H. Ghayoumi-Zadeh, "Miniaturized substrate integrated waveguide filter using fractal open complementary split-ring resonators," *International Journal of RF and Microwave Computer-Aided Engineering*, Vol. 28, No. 5, 21249, 1–7, May 2018.
12. Danaeian, M. and K. Afrooz, "Compact metamaterial unit-cell based on stepped-impedance resonator technique and its application to miniaturize substrate integrated waveguide filter and diplexer," *International Journal of RF and Microwave Computer Aided Engineering*, Vol. 29, No. 2, 21537, 1–9, Feb. 2018.